Centroidal Momentum Shaping for Task-Invariant Assistance: Preliminary Validation on a Bilateral Hip Exoskeleton

Miao Yu, Nikhila Krishnan, Thomas Holliday, Jesse Dean, and Ge Lv*

Abstract— **Existing control paradigms for lower-limb exoskeletons aim at replicating task-specific, subject-dependent reference kinematics, which overly constrain voluntary human motion. Individuals with voluntary control over their lower-extremities would likely benefit from the ability to choose their gait patterns freely while being assisted by exoskeletons during locomotion. In this paper, we propose a novel control paradigm and its implementation to alter an individual's Centroidal Momentum, i.e., a sum of projected limb momenta onto the human's center of mass, through tracking a dynamic reference Centroidal Momentum to provide consistent assistance across tasks. This reference Centroidal Momentum is defined based on a virtual reference model that has identical gaits self-selected by an individual and scaled inertial parameters, rather than reference trajectories. The resulting control strategy does not prescribe to any joint-level reference kinematics, providing flexibility for human users meanwhile providing assistance. We demonstrate experimental results on five non-disabled human subjects wearing a bilateral hip exoskeleton performing various walking tasks under different speed and incline/decline conditions. The results show that the generated exoskeleton assistance/resistance based on the proposed shaping strategy can reduce/increase the subjects' muscular efforts with the same set of control parameters, respectively, across the performed tasks.**

I. Introduction

Emerging powered lower-limb exoskeletons have demonstrated great potential in assisting humans for various activities [1]. Depending on the intended control and design goals, they can help bear the weight of extra loads [2], reduce energy expenditure [3], and restore normative gait kinematics [4]. The vast majority of existing control paradigms are trajectory-based that replicate reference kinematics for human user's joints [5], which are appropriate for individuals with neurological injuries that prevent voluntary generation of lower extremity motions [5]. For individuals with partial or full voluntary control over their lower extremities, control paradigms would ideally enable exoskeletons to provide assistance without confining to their preferred gaits for facilitating adaptability to various walking patterns [1].

Trajectory-free control approaches do not confine user's joint motion to specific reference kinematics, therefore allowing users greater flexibility in selecting their preferred gaits [1]. For instance, human muscle activations can be measured via Electromyographic (EMG) sensors and used as feedback for exoskeleton control design to assist human locomotion [6], [7]. However, performance of EMG sensors is susceptible and sensitive to measurement noises, placement of electrodes, and sweating [8]. Alternatively, predictive control paradigms can predict a user's walking patterns using plantar forces [9] to provide adaptive assistance without predefined trajectories. However, their effectiveness depends on prediction accuracy, and estimation errors can potentially lead to control failures [10]. Biological torque compensation is also widely used to augment voluntary motion, *e.g.*, Molinaro et al. proposed a deep learning-based method to estimate and compensate for biological joint torques in real-time [11]. However, these methods usually require extensive training data that could be difficult to obtain.

Recent advancements in energetic control methods have started to emphasize task invariance. In particular, energy shaping and passivity-based control methods [12]–[14] can enable exoskeletons to provide task-invariant assistance through dynamically altering human body energetics. While independent of reference trajectories, such methods require the solution of matching conditions to determine achievable closed-loop dynamics in the case of underactuation [13], which can be very challenging to obtain given varying degrees of underactuation during human locomotion. Although there exist other trajectory-independent, energetic control paradigms, they are specifically proposed for dedicated tasks such as sit-to-stand [15], stair ascent [16], or level-ground walking [3]. It remains unclear if these control paradigms can still demonstrate the same efficacy when translated to continuously varying daily activities.

As a commonly used metric in locomotion [17], Centroidal Momentum (CM), the sum of projected segmental momenta onto a robot's Center of Mass (CoM) [18], are often used in the control design for both bipeds and quadrupeds [17], [19]. CM has also been used as an index to evaluate the stability of human gaits [20], performance of balance recovery strategies [21], and incorporated in models that predict human CoM trajectory during sit-to-stand motion [22]. CM is consistently represented as a six-dimensional vector in 3D space regardless of biped models or walking gaits [18], which can be advantageous in designing control strategies. As long as the exoskeleton actuators span three anatomical planes, we can guarantee the existence of a control law to alter a human's CM even for underactuated systems. Control allocation (*i.e.*, achieving a desired CM with specific actuators) can also be realized, which is usually feasible when the

This work was supported by the National Science Foundation under Award 2340261. The content is solely the responsibility of the authors and does not necessarily represent the official views of the National Science Foundation.

* indicates corresponding author.

M. Yu, N. Krishnan, T. Holliday, and G. Lv are with the Department of Mechanical Engineering, Clemson University, Clemson, SC 29634, USA. {myu2, nikhila, tnholli, glv}@clemson.edu

J. Dean is with the Department of Rehabilitation Sciences, Medical University of South Carolina, Charleston, SC 29425, USA. deaje@musc.edu

system is overactuated [23]. Finally, altering a human's CM via an exoskeleton does not prescribe to joint-level reference kinematics, which has the potential to generate task-invariant assistance and promote voluntary human motion.

In this paper, we propose a control method (called CM shaping) to alter a human's CM for providing task-invariant assistance. The control law is yielded through tracking the desired CM based on a virtual reference model, whose joint kinematics are identical to an individual's self-selected gaits and limb inertial parameters are scaled versions of the individual's parameters. Through tracking this reference CM via exoskeleton actuators, we can mimic behaviors of the virtual reference model that has reduced/increased body weight compared to the human user (Fig. 1). We adopted a nonlinear disturbance observer (NDO) to estimate human joint torques and utilize this information in the overall control design. We implemented the proposed shaping strategy on a powered bilateral hip exoskeleton with highly backdrivable actuators, and conducted experiments with five non-disabled participants performing various walking tasks under different combinations of speeds and inclines/declines. Preliminary Experimental results demonstrate that the proposed CM shaping strategy generates assistance/resistance to reduce/increase muscular efforts across tasks.

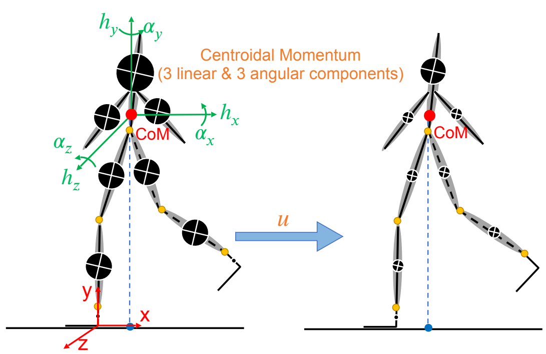

Fig. 1: Through shaping the CM of an individual via exoskeleton torque u, we can mimic the CM of a lighter person (right) for possible gait benefits.

II. Dynamics & Control Method

A. Biped Dynamics

We model a human wearing an exoskeleton as one whole biped and express its Euler-Lagrange dynamics as [24]

$$M\ddot{q}+C\dot{q}+N+A^T\lambda=\tau, \tag{1}$$

where n denotes the number of degrees of freedom (DoFs), $q\in\mathbb{R}^{\mathrm{n}}$ is the configuration vector that will be specified in Sec. IV, $M\in\mathbb{R}^{\mathrm{n}\times\mathrm{n}}$ is the positive-definite inertia matrix, $C\in\mathbb{R}^{\mathrm{n}\times\mathrm{n}}$ is the Coriolis/centrifugal matrix, and $N\in\mathbb{R}^{\mathrm{n}}$ denotes the gravitational force vector. The constraint matrix A, defined as the gradient of holonomic constraint functions, maps the ground reaction force vector $\lambda=\hat{\lambda}+\check{\lambda}\tau$ into the overall dynamics, where $\hat{\lambda}=W(\dot{A}\dot{q}-AM^{-1}N)$, $W=(AM^{-1}A^T)^{-1}$, and $\check{\lambda}=WAM^{-1}$ [24]. All inertial parameters in these matrices combine the human and exoskeleton values. The overall torque τ sums up two parts: the human joint torque vector τ_{hum} and the exoskeleton input $\tau_{\mathrm{exo}}=Bu$, where $B=(0_{\mathrm{p}\times\mathrm{n-p}},\ I_{\mathrm{p}\times\mathrm{p}})^T\in\mathbb{R}^{\mathrm{n}\times\mathrm{p}}$ is the mapping matrix for the exoskeleton torque $u\in\mathbb{R}^{\mathrm{p}}$.

B. Centroidal Momentum of the Biped

For a multi-link biped, the velocity vector v_G of each biped link with respect to its body frame is given as

$$v_G=J_G\dot{q}\in\mathbb{R}^{6\mathrm{j}},\quad J_G=[J_1^T,J_2^T,\cdots,J_{\mathrm{j}}^T]^T, \tag{2}$$

where $J_G\in\mathbb{R}^{6\mathrm{j}\times\mathrm{n}}$ is the system Jacobian matrix composed of body Jacobian matrices $J_i\in\mathbb{R}^{6\times\mathrm{n}}$, $i\in\{1,2,\cdots,\mathrm{j}\}$ for all j links [24]. The body momentum vector $h_{\mathrm{body}}\in\mathbb{R}^{6\mathrm{j}}$ that contains the body momentum of each link is then given as

$$h_{\mathrm{body}}=I_G v_G,\quad I_G=\mathrm{diag}\{I_{G1},I_{G2},\cdots,I_{Gj}\}, \tag{3}$$

where $I_G\in\mathbb{R}^{6\mathrm{j}\times6\mathrm{j}}$ is composed of inertia tensor matrices $I_{Gi}=\mathrm{diag}\{m_i\cdot I_{3\times3},\ I_i\cdot I_{3\times3}\}\in\mathbb{R}^{6\times6}$, $i\in\{1,2,3,\cdots,\mathrm{j}\}$ with m_i and I_i being the mass and moment of inertia of the i-th link, respectively. Finally, we project the body momenta vector h_{body} onto the biped's CoM to yield the CM as

$$h_G=X_G^T h_{\mathrm{body}}\in\mathbb{R}^6, \tag{4}$$

where $X_G\in\mathbb{R}^{6\mathrm{j}\times6}$ is the system adjoint transformation matrix [18]. Substituting (2) and (3) into (4), the CM of a multi-link biped can be expressed as

$$h_G=X_G^T I_G J_G\dot{q}:=A_G\dot{q}, \tag{5}$$

where $A_G=X_G^T I_G J_G\in\mathbb{R}^{6\times\mathrm{n}}$ [18].

C. Centroidal Momentum Shaping

We propose the following relationship between reference CM h_G^{ref}, h_G, and their derivatives as:

$$\dot{h}_G^{\mathrm{ref}}-\dot{h}_G+K_p(h_G^{\mathrm{ref}}-h_G)=0, \tag{6}$$

where $K_p\in\mathbb{R}^{6\times6}$ is a positive-definite diagonal matrix. We propose this definition to track the change rate of h_G^{ref} meanwhile minimizing the difference between h_G and h_G^{ref}, which is generated only after a human starts walking. Similar to following a target vehicle with varying speeds, we hope to achieve the same velocity for the follower vehicle rather than a desired position over time. Taking the time derivative of h_G^{ref} yields

$$h_G^{\mathrm{ref}}=A_G^{\mathrm{ref}}\dot{q},\quad \dot{h}_G^{\mathrm{ref}}=\dot{A}_G^{\mathrm{ref}}\dot{q}+A_G^{\mathrm{ref}}\ddot{q}^{\mathrm{ref}}, \tag{7}$$

where $\ddot{q}^{\mathrm{ref}}$ in (7) can be obtained from a virtual reference model

$$M^{\mathrm{ref}}\ddot{q}^{\mathrm{ref}}+C^{\mathrm{ref}}\dot{q}+N^{\mathrm{ref}}+A^T\lambda^{\mathrm{ref}}=\tau_{\mathrm{hum}}. \tag{8}$$

The matrices M^{ref}, C^{ref}, N^{ref}, and λ^{ref} in (8) are defined similarly to the ones in (1) but with m_i and I_i scaled $k_i\in\mathbb{R}^+$ times, *i.e.*, $m_i^{\mathrm{ref}}=k_i m_i$ and $I_i^{\mathrm{ref}}=k_i I_i$. Note that this virtual reference model shares the same joint kinematics as (1), *i.e.*, both models have identical gaits. Intuitively, selecting $k_i<1$ and $k_i>1$ will generate assistance and resistance, respectively, as the reference CM will be defined to reflect behaviors of a heavier or a lighter individual. Equating $\dot{h}_G$ in (6) with $\dot{A}_G\dot{q}+A_G\ddot{q}$, we obtain

$$\dot{h}_G^{\text{ref}} - A_G\ddot{q} - \dot{A}_G\dot{q} + K_p(A_G^{\text{ref}}\dot{q} - A_G\dot{q}) = 0. \tag{9}$$

In this paper, the hip exoskeleton we used (to be introduced later in Sec. III) is only equipped with sagittal-plane actuators to assist hip flexion/extension. With this limitation, the CM's linear component along the z-axis, and the angular momenta around x and y axes are zeros. Therefore, A_G contains only three non-zero rows that can be shaped, which further simplifies (9) into three equivalent equations. If an exoskeleton has more than three actuators in the sagittal plane, then there exists an infinite amount of solutions to the control law u that can alter linear components in x-y plane and the angular momentum around the z axis. We can specify a solution via an optimization procedure:

$$\begin{aligned} \min_{u} \quad & u^T W u \\ \text{s.t.} \quad & \dot{h}_G^{\text{ref}} - A_G\ddot{q} - \dot{A}_G\dot{q} + K_p(A_G^{\text{ref}}\dot{q} - A_G\dot{q}) = 0, \\ & u_{\min} \leq ||u||_2 \leq u_{\max}, \end{aligned}$$

where $W \in \mathbb{R}^{\text{p}\times\text{p}}$ is a diagonal, positive-definite weight matrix, $u_{\min}$, $u_{\max} \in \mathbb{R}$ are the lower and upper control torque bounds, respectively. The objective function is selected as $u^T W u$ to minimize torques exerted by the exoskeleton actuators for energy efficient solutions. Additionally, the weight matrix W can be adjusted to achieve control allocation for specific joints. The above optimization problem can be solved by using the Lagrange multiplier method [25].

Let $\eta \in \mathbb{R}^{\text{m}}$ be the Lagrange multiplier with m being the number of non-zero elements to be shaped in CM, the Lagrangian $\mathcal{L}$ is defined as

$$\mathcal{L}(u,\eta) = u^T W u - \eta^T(-A_G\ddot{q} + Y). \tag{10}$$

where $Y = -\dot{A}_G\dot{q} + \dot{h}_G^{\text{ref}} + K_p(A_G^{\text{ref}}\dot{q} - A_G\dot{q})$. Setting the gradient of $\mathcal{L}$ with respect to u and η to zero, *i.e.*,

$$\frac{\partial \mathcal{L}}{\partial u} = 0, \quad \frac{\partial \mathcal{L}}{\partial \eta} = 0, \tag{11}$$

the CM shaping law is obtained as

$$u^* = W^{-1}D^T(DW^{-1}D^T)^{-1}(A_G M^{-1} H + Y), \tag{12}$$

where $D = A_G M^{-1} B_\lambda$, $B_\lambda = B - A^T\check{\lambda}$, $H = C\dot{q} + N + A^T\hat{\lambda} - \tilde{\tau}_{\text{hum}}$, and $\tilde{\tau}_{\text{hum}} = (I - A^T\check{\lambda})\tau_{\text{hum}}$.

D. Nonlinear Disturbance Observer

The proposed CM shaping strategy (12) requires knowledge of τ_{hum}, which can be difficult to measure in practice. We modify an existing model-based NDO [26] to estimate human joint torques based on angular information. The required sensors for measurements will be discussed in Sec. III-B. Defining $z = M^{-1}\tilde{\tau}_{\text{hum}}$ as the term that needs to be estimated and left-multiplying M^{-1} at both sides of (1), we have

$$z = \ddot{q} + M^{-1}C\dot{q} + M^{-1}N + M^{-1}A^T\hat{\lambda} - M^{-1}B_\lambda u. \tag{13}$$

Denoting $\hat{z}$ as the estimate for z and $e = z - \hat{z}$ as the estimation error, we have [27]:

$$\dot{\hat{z}} = Le = L(z - \hat{z}), \tag{14}$$

where $L \in \mathbb{R}^{\text{n}\times\text{n}}$ can be chosen as a positive-definite, diagonal matrix to guarantee uniformly ultimate boundness and fast convergence of e [27] that is governed by

$$\dot{e} = \dot{z} - \dot{\hat{z}} = \dot{z} - Le. \tag{15}$$

We will demonstrate the performance of the proposed NDO later in Sec. IV-D.

III. Bilateral Hip Exoskeleton System

To demonstrate efficacy of the proposed method, we implemented the CM shaping strategy (12) on a bilateral, powered hip exoskeleton with highly backdrivable (*i.e.*, low mechanical impedance) actuators, with inertial measurement units (IMUs) mounted on thigh and shank for kinematic measurements (Fig. 2, left). In this section, we introduce the overall structure of the exoskeleton control system.

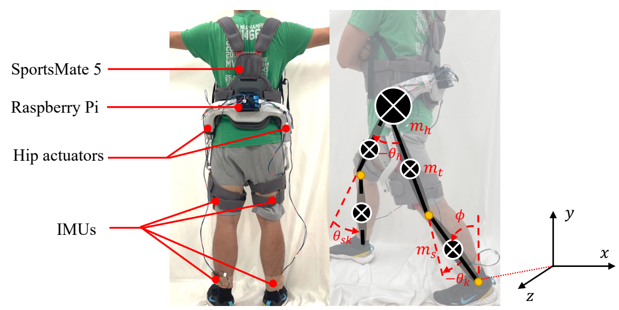

Fig. 2: A subject wearing SportsMate 5 with IMUs (left) and the 4-DoF experimental model (right).

A. SportsMate 5 Exoskeleton

SportsMate 5 (Enhanced Power Technology Co., Ltd., Shenzhen, China) has two brushless direct current motors that can produce 7.5 Nm continuous torque (22.5 Nm peak torque) after a 25:1 transmission ratio. The actuators are highly backdrivable (0.096 Nm backdrive torque) to allow voluntary human motion. It also includes two magnetic absolute joint encoders (with embedded Kalman filters) and current sensors to realize closed-loop torque control at 400 Hz on a GD32F303RE microprocessor (ARM Cortex-M4, 120 MHz, 512 kB ROM, 64 kB RAM). The microprocessor is equipped with a UART port and a Bluetooth module to allow for external communication. The exoskeleton weighs about 3.2 kg including a 3200 mAh onboard Lithium battery.

B. Human Kinematics Measurement

To measure human limb kinematics for control implementation, we integrated four IMU sensors (NGIMU, x-io Technologies Limited, Bristol, UK) at subject's shanks and thighs (Fig. 2, left) to measure human joint kinematics (will be specified in Sec. IV-A). The IMUs are embedded with an AHRS fusion algorithm [28] to smooth out its output, which is then sent to a Raspberry Pi 4B (8GB LPDDR4-3200

SDRAM, Quad core Cortex-A72 64-bit SoC, 1.8 GHz) via the UART protocol. Once angular positions are measured, we take numerical derivatives to obtain the corresponding angular velocities and accelerations, where a moving average filter with window size of 71 was applied to attenuate noises in accelerations.

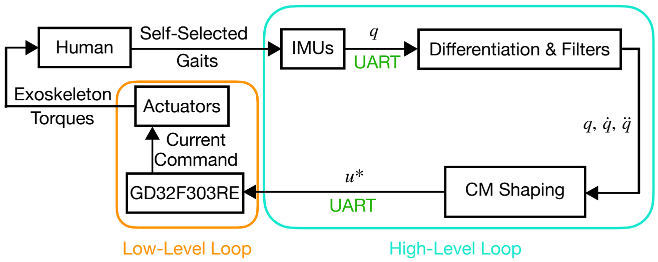

Fig. 3: Overall hardware structure of the exoskeleton system.

C. Control Architecture

The overall control hierarchy in Fig. 3 consists of two loops: a high-level loop that computes u^* from (12) and a low-level loop that regulates the desired torques. Due to limited computation capability of SportsMate 5's default microprocessor, we used a Raspberry Pi to receive real-time IMU feedback, compute command torque in C at about 150 Hz, and transmit it to SportsMate 5's microprocessor via serial communication. The exoskeleton's embedded motor driver (ER-Driver) will regulate actuator currents to achieve the desired torque based on a torque constant of 0.083 Nm/A. Note that we can update control law on the Raspberry Pi at 550 Hz, but we deliberately reduced the calculation speed to match SportsMate 5's communication frequency.

IV. Experimental Study

In this section, we present implementation of the proposed CM shaping strategy and present experimental results on five non-disabled human subjects performing various walking tasks with different combinations of speeds and inclines/declines.

A. 4-DoF Experimental Biped Model

SportsMate 5 is equipped with two hip actuators in the sagittal plane to assist hip flexion/extension, which is unlikely to have direct impacts on human ankle joints. We therefore adopted a 4-DoF point-feet biped model [29] to derive u^* for experiments considering the computational capabilities of the onboard computing units. The configuration vector of the model is given as $q_{\text{exp}} = (\phi, \theta_{\text{k}}, \theta_{\text{h}}, \theta_{\text{sk}})^T \in \mathbb{R}^4$ (Fig. 2, right) and was measured by four IMU sensors attached at the shank and thigh of both legs. To avoid using additional force sensors on human feet, we set $\hat{\lambda} = 0$ in (12) thus $B_\lambda = B$, $\tilde{\tau}_{\text{hum}} = \tau_{\text{hum}}$. Inertial terms of humans are estimated following the methods in [30].

The 4-DoF experimental model is defined based on an inertial reference frame (IRF) located at an individual's stance foot. To address the IRF changes during stance leg transitions, we defined two identical 4-DoF models as shown in Fig. 2, each anchored to one foot. During experiments, the model associated with the current stance leg will be used to compute u^* and then sent to the leg's actuator. We approximate stance leg transitions by detecting the hip angular velocity, *i.e.*, its value reaching zero marks the onset of the double support phase [31]. Actuator torques were saturated at ± 10 Nm to ensure safety, and we assumed each actuator contributed equally to the torque command u^* but in opposite directions throughout the gait cycle [32].

B. Experimental Protocol

We enrolled 5 non-disabled human subjects (s1: male, 84.2 kg, 1.83 m; s2: male, 60.4 kg, 1.65 m; s2: female, 60.1 kg, 1.70 m; s4: male, 62.6 kg, 1.76 m; s5: female, 63 kg, 1.62 m) for experiments. The experimental protocol was approved by the Institutional Review Board of Clemson University (IRB2022-0322), and subject consent was obtained prior to the start of all experiments. All experiments were conducted on an instrumented treadmill (Bertec Corporation, OH, US).

Before we started extensive data collection, we performed preliminary testing on s1 to assess the effects of shaping different components of CM (linear components along x and y axes, and angular component around the z axis) and the associated shaping parameters. To ensure safety, only level-ground walking was performed, and the speed was set to 0.8 m/s. We selected four values for k_i as $\{0.85,\ 0.95,\ 1.1,\ 1.2\}$. The selected parameters were then used in the subsequent experiments for data collection on s2 to s5 while ensuring their comfort.

The main experiments for s2 to s5 were divided into 8 groups, and each group contained three control modes, *i.e.*, passive (P, $k_i = 1$, zero actuator torques), resistive (R, $k_i > 1$), and assistive (A, $k_i < 1$), respectively. The speeds and incline conditions for each group are summarized in Table I, where "LG", "RA", and "RD" denote level ground walking, ramp ascent (5°), and ramp descent (5°). For each condition and control mode, data from 20 steady-state steps were recorded within the first minute since the beginning of each trial. In all experiments, we set $K_p = 10$ and $L = 100 \cdot I_{4\times 4}$ for the NDO, chosen via trial-and-error to balance convergence speed and reasonable actuator torques that are within limits. For assistive/resistive trails, subjects were not informed with the underlying control mode. Instead, we asked them to provide feedback on their perceived control modes afterward. All recorded data was cropped into gait cycles by heel strikes detected by the treadmill's embedded force plates.

We also recorded muscle activations of Rectus Femoris (RF), Biceps Femoris (BF), and Gluteus Medius (GM) via EMG sensors (Trigno Avanti Sensor, Delsys Inc., MA, USA), where RF functions as a hip flexor, and BF, GM as hip extensors [33]. The EMG data were first filtered by a fourth-order bandpass filter (20-500 Hz), rectified, then by a 6 Hz low-pass filter and rectified [34]. The EMG data were then normalized with respect to the maximum peak of the ensemble averages (across repetitions) of three control modes within each group. This converted the EMG signals to a percentage of the peak filtered EMG value during the trials. After normalizing the EMG to peak EMG (%), we calculated the integral with respect to gait cycle to represent muscular effort.

TABLE I: Experiment Scenarios per Subject

Group	1	2	3	4	5	6	7	8
Speed (m/s)	0.8	1	1.2	0.8	1	1.2	0.8	1
Condition	LG	LG	LG	RA	RA	RA	RD	RD

C. Results on s1 & Parameter Selection

For preliminary testing on s1, we recorded exoskeleton torques, CM, and muscle activities of RF, BF, GM during 20 steady steps, where the results are shown in Figs. 4 to 7. In all figures throughout the paper, 0% of the gait cycle corresponds to heel strike of the stance leg, and positive/negative torque directions indicate hip flexion/extension, respectively.

The control torques that shape the linear components along x and y axes and the angular momentum around the z axis with $k_i = 0.85$ are shown in Fig. 4. All control torques exhibit similar amplitudes and shapes, except for the one shaping linear momentum along the y-axis that has more sudden changes and vibrations. This may be due to the small y-axis CoM displacement compared to the x-axis [35], making control torque more sensitive to measurement noise. In addition, Fig. 5 shows that a smaller value of k_i (further away from 1) results in greater value of torques. Fig. 6 further demonstrates s1's linear CM along the y-axis, with the exoskeleton shaping the linear components along x and y axes and the angular momentum around the z axis. Overall, all three shaping strategies preserve the shape of s1's linear CM but alter its magnitude, indicating that the proposed shaping strategy is able to allow for voluntary motion.

Fig. 7 compares the EMG result of left BF under three different assistive shaping strategies (top) and left GM with varying parameters for shaping the linear component in the x direction (bottom). We can see that shaping the linear component of CM along x-axis brings relative lower muscle activation in assistive mode compared to shaping the other two components. Moreover, when shaping the linear component along x-axis, compared to passive walking, the assistive mode resulted in lower muscle efforts, whereas the resistive mode resulted in higher muscle activity, which matches the design expectation. Based on the preliminary test results on s1, we chose to shape the linear component along x-axis (which aligns with the primary direction of human locomotion) and k_i to be 0.85 (`A`) and 1.2 (`R`) for experiments.

D. Results on s2 to s5

The experimental results s2 to s5 are shown in Figs. 8 to 12. We present results for selected subjects and tasks due to their overall similarity, and encode results in the paper following the format: `(Result Type; Group Number (G); Subject Code (s); Specifics)`. All assistive/resistive trials were successfully recognized by the subjects via a survey after data collection, except for 2 trials (out of 96 trials). The estimated hip torques using NDO (Fig. 8) demonstrate consistent shapes in all control modes for s4, which closely match the ones from Winter's dataset

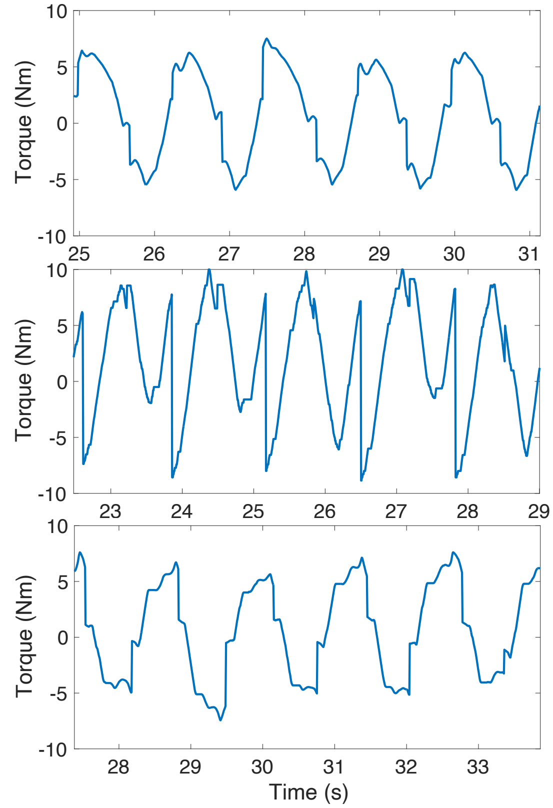

Fig. 4: Control torques with shaping the linear component along x-axis (top), linear component along the y-axis (middle), and z-axis angular component (bottom), all with $k_i = 0.85$.

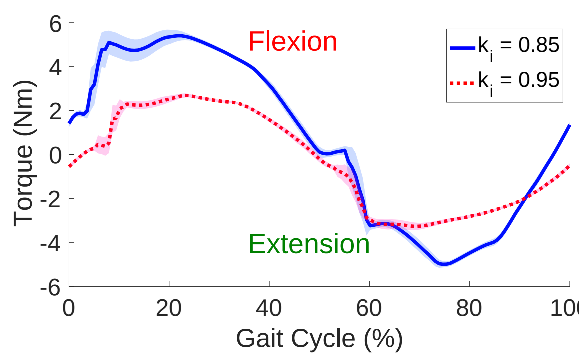

Fig. 5: Mean ± 0.5·SD of control torques that shape s1's linear CM (x-axis) with $k_i = 0.85$ and 0.95.

[31] in magnitude and shape, supporting the feasibility of the proposed NDO. Minor discrepancies, including a phase lead and shape variations, stem from the simplified 4-DoF experimental model for experiments, which does not fully capture human motion. Additionally, the model combines both hip joints into one, therefore the estimated torques represent their combined effect. Despite these limitations, we will still see benefits of the proposed shaping strategy on muscular efforts later.

The command and tracking torques are shown in Fig. 9. We can see that the actuator system was able to accurately track the generated torque commands. In Fig. 11, CM's magnitude, particularly the angular component, is lower in the resistive

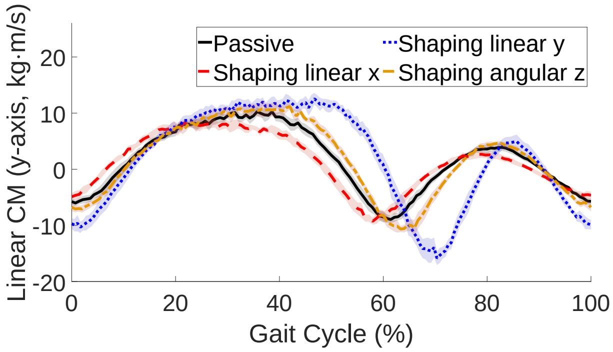

Fig. 6: Mean $\pm$ 0.5·SD of s1's linear component (y-axis) when shaping three different components with $k_i = 0.85$.

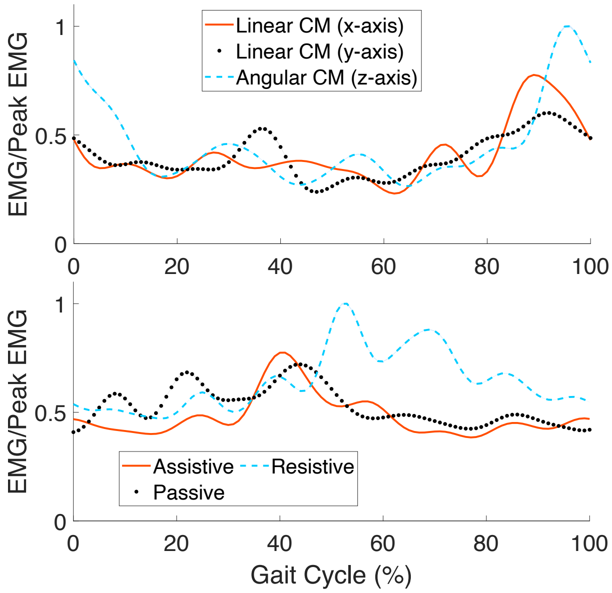

Fig. 7: Mean $\pm$ 1·SD EMG results of left BF when shaping three different components with $k_i = 0.85$ (top) and left GM with $k_i = 0.85$, 1, and 1.2 (bottom).

mode compared to the assistive mode. Because resistive strategies aim to mimic a heavier person, with human joint inputs from the same subject and the constant treadmill speeds within each mode, the resulting CM is greater accompanied by increased muscular efforts.

EMG results of representative subjects are shown in Fig. 10, as other exhibit similar patterns. Resistive mode in general resulted in higher EMG values thus increased muscle efforts, in terms of either maximum peak, *e.g.*, (G3; s2; RF_L), or prolonged muscular utilization such as (G3; s2; GM_L). On the contrary, assistive mode reduced muscle activities, *e.g.*, (G3; s2; GM_L) and (G4; s4; RF_L), which aligns with the subjects' qualitative feedback that assistive mode results in less effort, especially in the tasks that typically demand more muscle effort such as RA (G4 in Fig. 10).

Some assistive trials show close EMG activity in certain muscles compared to passive mode, likely due to two reasons. The subjects in this study had no prior experiences with the exoskeleton, therefore muscular efforts could be

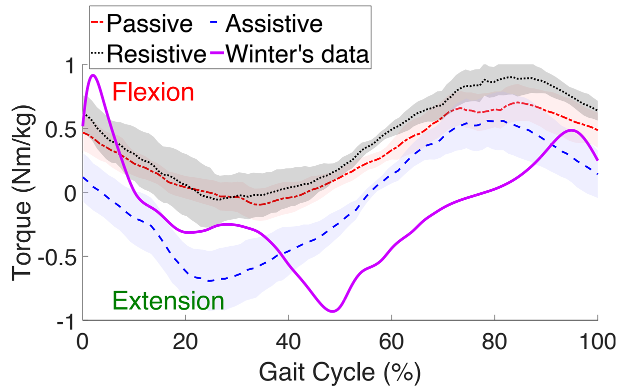

Fig. 8: Mean $\pm$ 0.5·SD of the estimated hip torques; G3; s4.

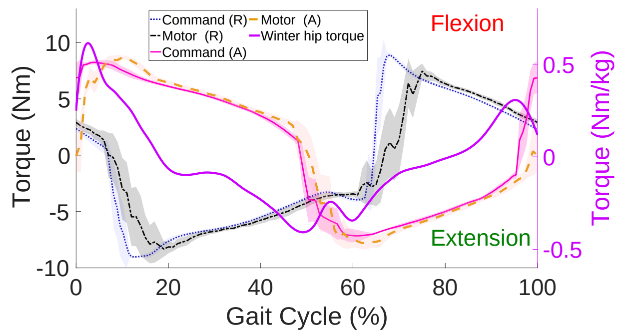

Fig. 9: Mean $\pm$ 0.5·SD of command and tracking actuator torques; G2; s2.

further reduced with improved co-adaptation over time. The control parameters were fixed across subjects, which may not perfectly align with all subject's preferences. For example, (G2; s5; RF_L) shows a delayed onset compared to other subjects, closely coinciding with the torque transition from flexion to extension that could lead to higher EMG peaks. During the first half of a gait cycle, the assistive mode provides flexion torques and this coincides with the onset of RF in Fig. 10 that functions as a hip flexor. Similarly, the extension torque during the second half of the gait cycle coincides with the onset of BF in Fig. 10.

Another interesting observation is that in RD trials, both assistive and resistive modes result in lower muscular efforts, *e.g.*, (G8; s4; RF_R) compared to passive mode. According to subject feedback, these two modes reduced muscle activities differently. In assistive mode, similar to LG and RA trials, the proposed shaping method provided control aligned with the subjects' self-selected motion, which led to reduced muscle activities. In resistive trials, subjects reported that resistive torques helped regulate their pace, preventing excessive speed or step length, making them feel more "secure" and potentially lowering muscular efforts.

Finally, Fig. 12 presents the ratio of the integrated EMG over a gait cycle (IEMG) between assistive and passive mode, or resistive and passive mode. A ratio greater than one indicates greater muscular effort than passive gait. Compared to the passive mode, each subject's GM has consistently lower/higher IEMG ratios during most of the assistive/resistive

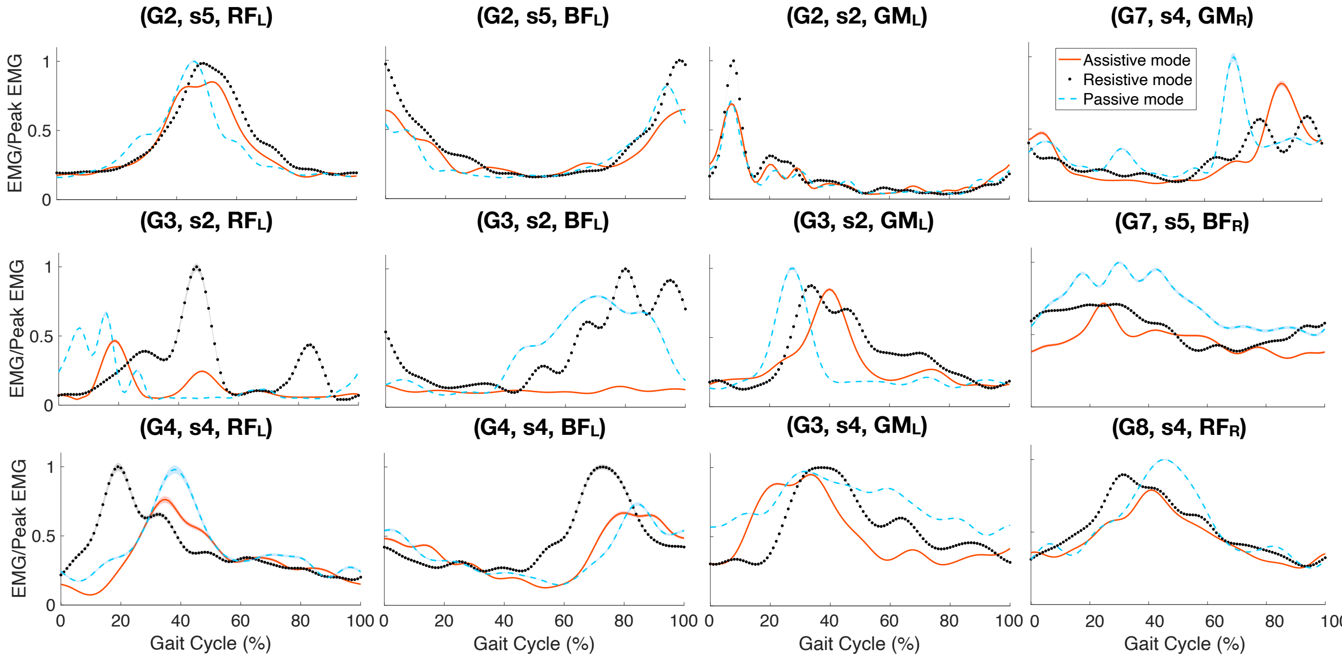

Fig. 10: Mean $\pm$ 1·SD EMG of s2 to s5 performing different tasks. Subscripts "L" and "R" indicate left and right, respectively.

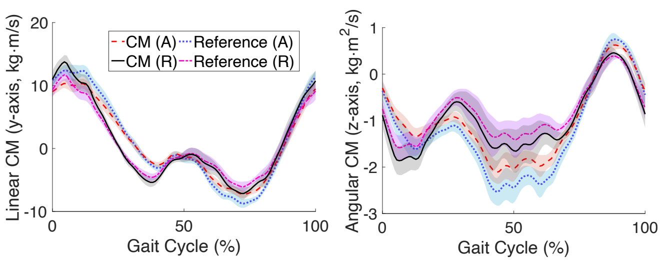

Fig. 11: Mean $\pm$ 0.5·SD of actual and reference CM, G2, s3, left: y-axis (linear), right: z-axis (angular).

modes, respectively. It is evident that almost all muscles have increased effort in all resistive trials. This aligns with the subjects' feedback that during their perceived resistive modes, they felt harder to walk, especially during RA (G4 to G6).

V. Conclusions

In this paper, we proposed a task-invariant CM shaping paradigm that assists/resists human locomotion by altering the human's CM. By defining a virtual reference model based on the human user's self-selected gaits and scaled inertial parameters, the proposed shaping strategy tracks the reference CM to dynamically mimic the gaits of a lighter/heavier person. Experimental results on five non-disabled subjects performing different walking tasks demonstrated reduction/increments in muscle activations with assistance/resistance, respectively, all with the same set of control gains. Nearly all subjects were able to recognize the underlying strategy without knowing the control modes. These results support extending this control paradigm to individuals with limited voluntary control of safe, efficient lower-limb motions. Future work includes investigating the effects of different CM shaping parameters (K_p, k_i) and incorporating learning techniques to customize exoskeleton assistance for different users.

Acknowledgment

The authors thank Hamdan Sarvathullah and Shenbao Wang for their help on hardware implementation.

References

[1] R. Baud, A. R. Manzoori, A. Ijspeert, and M. Bouri, "Review of control strategies for lower-limb exoskeletons to assist gait," *J. NeuroEng. Rehabil.*, vol. 18, no. 1, pp. 1–34, 2021.

[2] T. Wang, Y. Zhu, T. Zheng, D. Sui, S. Zhao, and J. Zhao, "Palexo: A parallel actuated lower limb exoskeleton for high-load carrying," *IEEE Access*, vol. 8, pp. 67 250–67 262, 2020.

[3] Q. Zhang, V. Nalam, X. Tu, M. Li, J. Si, M. D. Lewek, and H. H. Huang, "Imposing healthy hip motion pattern and range by exoskeleton control for individualized assistance," *IEEE Robot. Autom. Lett.*, vol. 7, no. 4, pp. 11 126–11 133, 2022.

[4] B. Johnson and M. Goldfarb, "A preliminary study on the feasibility of using a knee exoskeleton to reduce crouch gait in an adult with cerebral palsy," in *Int. Conf. Biomed. Robot. Biomechatronics*. IEEE, 2020, pp. 48–53.

[5] T. Yan, M. Cempini, C. M. Oddo, and N. Vitiello, "Review of assistive strategies in powered lower-limb orthoses and exoskeletons," *Robot. Auton. Syst.*, vol. 64, pp. 120–136, 2015.

[6] H. Hsu, I. Kang, and A. J. Young, "Design and evaluation of a proportional myoelectric controller for hip exoskeletons during walking," in *Dyn. Syst. Control Conf.*, vol. 51890. ASME, 2018, p. V001T13A005.

[7] S. Y. Gordleeva, S. A. Lobov, N. A. Grigorev, A. O. Savosenkov, M. O. Shamshin, M. V. Lukoyanov, M. A. Khoruzhko, and V. B. Kazantsev, "Real-time EEG–EMG human–machine interface-based control system for a lower-limb exoskeleton," *IEEE Access*, vol. 8, pp. 84 070–84 081, 2020.

[8] A. J. Young and D. P. Ferris, "State of the art and future directions for lower limb robotic exoskeletons," *IEEE Trans. Neural Syst. Rehabil. Eng.*, vol. 25, no. 2, pp. 171–182, 2016.

[9] M. Ding, M. Nagashima, S.-G. Cho, J. Takamatsu, and T. Ogasawara, "Control of walking assist exoskeleton with time-delay based on the prediction of plantar force," *IEEE Access*, vol. 8, pp. 138 642–138 651, 2020.

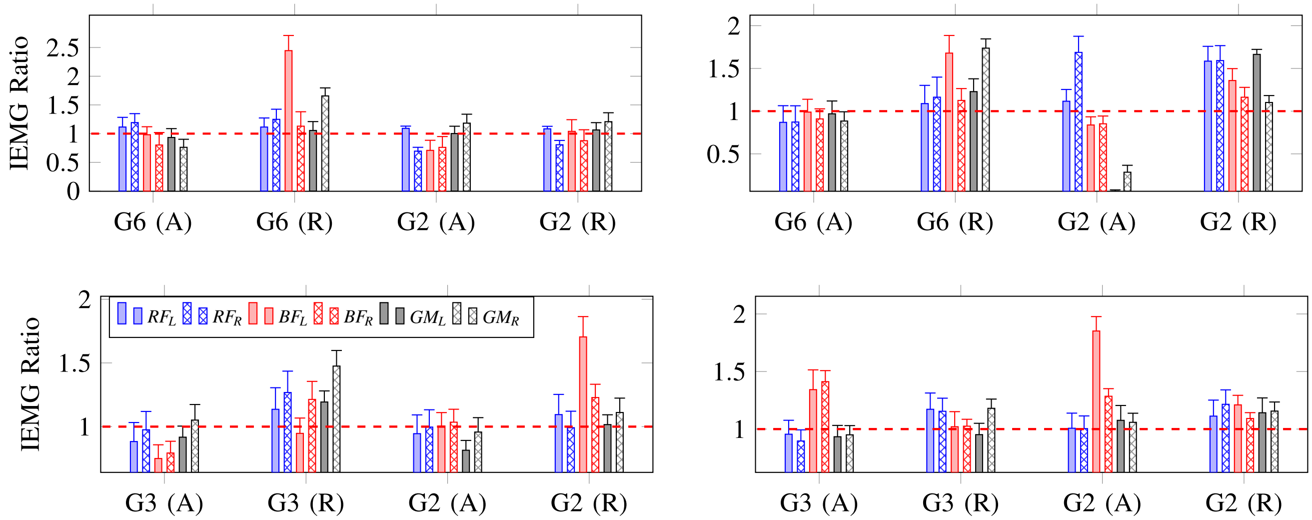

Fig. 12: Mean + 1·SD of IEMG ratio of s2 to s5 (top-left to bottom-right). Within each graph, the first and second `A-R` pairs show the best and average results for each subject.

[10] Y. Sun, Y. Tang, J. Zheng, D. Dong, X. Chen, and L. Bai, "From sensing to control of lower limb exoskeleton: A systematic review," *Annu. Rev. Control*, vol. 53, pp. 83–96, 2022.

[11] D. D. Molinaro, K. L. Scherpereel, E. B. Schonhaut, G. Evangelopoulos, M. K. Shepherd, and A. J. Young, "Task-agnostic exoskeleton control via biological joint moment estimation," *Nature*, vol. 635, no. 8038, pp. 337–344, 2024.

[12] J. Lin, N. V. Divekar, G. Lv, and R. D. Gregg, "Optimal task-invariant energetic control for a knee-ankle exoskeleton," *Control Syst. Lett.*, vol. 5, no. 5, pp. 1711–1716, 2020.

[13] G. Lv, H. Zhu, and R. D. Gregg, "On the design and control of highly backdrivable lower-limb exoskeletons: A discussion of past and ongoing work," *IEEE Control Syst. Mag.*, vol. 38, no. 6, pp. 88–113, 2018.

[14] G. Lv, J. Lin, and R. D. Gregg, "Trajectory-free control of lower-limb exoskeletons through underactuated total energy shaping," *IEEE Access*, vol. 9, pp. 95 427–95 443, 2021.

[15] M. K. Shepherd and E. J. Rouse, "Design and validation of a torque-controllable knee exoskeleton for sit-to-stand assistance," *IEEE/ASME Trans. Mechatron.*, vol. 22, no. 4, pp. 1695–1704, 2017.

[16] W. Ma, H. Cheng, R. Huang, and Q. Chen, "Gait planning with dynamic movement primitives for lower limb exoskeleton walking upstairs," in *IEEE Int. Conf. Robot. Biomim*, Dec. 2018, pp. 703–708.

[17] T. Koolen, S. Bertrand, G. Thomas, T. De Boer, T. Wu, J. Smith, J. Englsberger, and J. Pratt, "Design of a momentum-based control framework and application to the humanoid robot atlas," *Int. J. Humanoid Robot.*, vol. 13, no. 01, p. 1650007, 2016.

[18] D. E. Orin, A. Goswami, and S.-H. Lee, "Centroidal dynamics of a humanoid robot," *Auton. Robots*, vol. 35, no. 2, pp. 161–176, 2013.

[19] M. Liu, D. Qu, F. Xu, F. Zou, P. Di, and C. Tang, "Quadrupedal robots whole-body motion control based on centroidal momentum dynamics," *Appl. Sci.*, vol. 9, no. 7, p. 1335, 2019.

[20] J. H. Jung, L. V. Opheusden, P. Barralon, and J. F. Veneman, "Real time computation of centroidal momentum for the use as a stability index applicable to human walking with exoskeleton," in *Wearable Robotics: Challenges and Trends*. Springer, 2017, pp. 157–161.

[21] C. Bayon, A. Emmens, M. Afschrift, T. Van Wouwe, A. Keemink, H. Van Der Kooij, and E. Van Asseldonk, "Can momentum-based control predict human balance recovery strategies?" *IEEE Trans. Neural Syst. Rehabil. Eng.*, vol. 28, no. 9, pp. 2015–2024, 2020.

[22] G. Patil, L. Rigoli, M. J. Richardson, M. Kumar, and T. Lorenz, "Momentum-based trajectory planning for lower-limb exoskeletons supporting sit-to-stand transitions," *Int. J. Intell. Robot. Appl.*, vol. 2, no. 2, pp. 180–192, 2018.

[23] A. Casavola and E. Garone, "Fault-tolerant adaptive control allocation schemes for overactuated systems," *Int. J. Robust Nonlinear Control*, vol. 20, no. 17, pp. 1958–1980, 2010.

[24] R. M. Murray, Z. Li, and S. S. Sastry, *A mathematical introduction to robotic manipulation*. NW Boca Raton, FL: CRC press, 2017.

[25] M. Yu and G. Lv, "Task-invariant centroidal momentum shaping for lower-limb exoskeletons," in *Conf. Decis. Control*. IEEE, 2022, pp. 2054–2060.

[26] W.-H. Chen, D. J. Ballance, P. J. Gawthrop, and J. O'Reilly, "A nonlinear disturbance observer for robotic manipulators," *IEEE Trans. Ind. Electron.*, vol. 47, no. 4, pp. 932–938, 2000.

[27] H. K. Khalil, *Nonlinear systems; 3rd ed.* Upper Saddle River, NJ: Prentice-Hall, 2002.

[28] S. Madgwick *et al.*, "An efficient orientation filter for inertial and inertial/magnetic sensor arrays," *Report x-io and University of Bristol (UK)*, vol. 25, pp. 113–118, 2010.

[29] E. R. Westervelt, J. W. Grizzle, C. Chevallereau, J. H. Choi, and B. Morris, *Feedback control of dynamic bipedal robot locomotion*. NW Boca Raton, FL: CRC press, 2018.

[30] R. M. Enoka, *Neuromechanics of human movement*. Hum. Kinet., 2008.

[31] D. A. Winter, *Biomechanics and motor control of human movement*. John Wiley & Sons, 2009.

[32] J. Lee, M. E. Huber, and N. Hogan, "Gait entrainment to torque pulses from a hip exoskeleton robot," *Trans. Neural Syst. Rehabil. Eng.*, vol. 30, pp. 656–667, 2022.

[33] D. A. Neumann, "Kinesiology of the hip: a focus on muscular actions," *J Orthop Sports Phys Ther.*, vol. 40, no. 2, pp. 82–94, 2010.

[34] T. Parr, "Development of a novel predictive model and prosthetic system to assess dynamic leg length based gait biomechanics in lower limb prosthesis users," Ph.D. dissertation, Clemson University, 2023.

[35] L. Tesio and V. Rota, "The motion of body center of mass during walking: a review oriented to clinical applications," *Front. Neurol.*, vol. 10, p. 999, 2019.